Quasiparticle recombination in hotspots in superconducting current-carrying nanowires

A. G. Kozorezov,[1] C. Lambert,[1] F. Marsili,[2] M. J. Stevens,[3] V. B. Verma,[3] J. A. Stern,[2] R. Horansky,[3] S. Dyer,[3] S. Duff,[3] D. P. Pappas,[3] A. Lita,[3] M. D. Shaw,[2] R. P. Mirin,[3] and Sae Woo Nam[3]

[1]*Department of Physics, Lancaster University, Lancaster, United Kingdom*

[2]*Jet Propulsion Laboratory, California Institute of Technology, 4800 Oak Grove Dr., Pasadena, California 91109, USA*

[3]*National Institute of Standards and Technology, 325 Broadway, Boulder, Colorado 80305, USA*

(Received 7 May 2015; revised manuscript received 9 July 2015; published 6 August 2015)

We describe a kinetic model of recombination of nonequilibrium quasiparticles generated by single photon absorption in superconducting current-carrying nanowires. The model is developed to interpret two-photon detection experiments in which a single photon does not possess sufficient energy for breaking superconductivity at a fixed low bias current. We show that quasiparticle self-recombination in relaxing hotspots dominates diffusion expansion effects and explains the observed strong bias current, wavelength, and temperature dependencies of hotspot relaxation in tungsten silicide superconducting nanowire single-photon detectors.

DOI: 10.1103/PhysRevB.92.064504 PACS number(s): 74.40.Gh, 74.25.F−, 85.25.Oj, 74.25.Gz

I. INTRODUCTION

The detection mechanism of a superconducting nanowire single-photon detector (SNSPD) relies on the local photon-induced suppression of superconductivity [1]. This region of suppressed superconductivity is usually referred to as a hotspot (HS). Hotspot dynamics are crucially important for the operation of SNSPDs because they determine the spectral sensitivity [2] and limit the reset time of the detectors [3]. The formation and subsequent dynamics of hotspots play central roles in the detection mechanism. Despite significant progress in the development of SNSPDs, many fundamental questions remain open. These relate both to formation and evolution of a hotspot following the absorption of a photon and to the detection mechanism. Here we introduce a model that describes relaxation of strongly nonequilibrium distributions of interacting quasiparticles (QPs) and phonons inside a generated hotspot. We show that this model provides interpretation of recent two-photon experiments [4] describing in detail the evolution of relaxing hotspots. It quantitatively reproduces the measured current, wavelength, and temperature dependence of the hotspot relaxation time.

A recent experimental study of photodetection mechanisms in a superconducting nanowire single-photon detector [5] considers the four detection scenarios. The first is the normal-core hotspot model (a), where the photon energy creates a normal domain inside the superconductor, which the supercurrent must bypass. The second (b) is the diffusion-based hotspot model, where the nonequilibrium quasiparticles (QPs) diffuse outward from the point of absorption, creating a band of depleted (broken) superconductivity. The third (c) is the vortex nucleation model, where a vortex-antivortex pair is formed in the hotspot. This is a modification of model (a). Finally, in the vortex crossing model (d), either a vortex or a vortex-antivortex pair uses an area of weakened superconductivity to cross the wire and annihilate. This is a modification of the diffusion model (b), where superconductivity is not broken, while the detection mechanism is through photon-enhanced vortex unbinding. The main conclusion [5] is that the single photon detection experiment is consistent with a detection model (d) that relies on the vortex unbinding in the region of suppressed superconductivity [6–9].

By contrast, the characteristics and time evolution of the region of suppressed superconductivity in the hotspot forms the focus of this work. This important question was not addressed in detail earlier primarily because of the difficulty of separating the role of different factors in single photon experiments. In our recent work [4] the relaxation dynamics of hotspots were studied in the *two-photon detection* regime. This technique ideally suits the objective to study weakened superconductivity in the hotspot. In this situation the energy of a single photon is not sufficient to create a response pulse, and single photon detection efficiency is negligible. In the two-photon detection regime, the response pulse can be efficiently triggered only if two incident photons generate two hotspots overlapping spatially and temporally. Nonetheless following photon absorption a strongly nonequilibrium hotspot is formed. This exactly corresponds to the situation of scenario (b) above, where hotspot represents the volume where superconductivity is suppressed but not broken. Arrival of the second photon of the same energy but with variable time delay, t_D, relative to the first photon results in a detection click only provided that there is a significant spatial and temporal overlap of the two hotspots. The exact mechanism leading to a detection click is not important for understanding the dynamics of hotspot relaxation. The experiment is essentially a modification of the well-known pump-and-probe technique where the probe photon merely registers the state of relaxation of the hotspot, which was generated by the pump photon. Interpreting this experiment we therefore may concentrate on specific aspects of cooling dynamics of nonequilibrium distribution of QPs within the hotspot region in the current-carrying superconducting nanowire.

In Sec. II we give a description of the model, defining important stages of relaxing hotspots and introducing the main assumptions. Section III contains the results of a theoretical simulation of relaxation dynamics of hotspots in current-carrying superconducting nanowires. In Sec. IV, a comparison between theory and experiment is given, followed by a general discussion.

II. HOTSPOT IN A CURRENT-CARRYING SUPERCONDUCTING NANOWIRE

In typical SNSPDs, the electron diffusivity in nanowires in the normal state, D, is below 1 cm^2/s, and the parameter $k_F l \geqslant 1$, where k_F is the Fermi wave vector and l is the electron mean free path. Nanowires are strongly disordered, sometimes even being on the edge of a superconductor-insulator transition. Spectral and transport properties of strongly disordered superconductors on the edge of a superconductor-insulator transition are currently a topic of great interest both from experimental and theoretical points of view [10–12]. The transition is driven by the increase in the number of incoherent pairs at the expense of the ones that participate in the condensate. We assume that an SNSPD, in spite of being close to the transition, has its global superconductivity preserved. Under these circumstances the order parameter Δ in an SNSPD may exhibit strong local fluctuations on the scale of the order parameter, indicating a spontaneously formed inhomogeneity [10]. In a typical hotspot, $L_{HS} \gg \xi_0$, where L_{HS} is the linear size of the hotspot and ξ_0 is the coherence length. For this reason we will consider nonequilibrium dynamics and transport in an SNSPD in the model of a dirty BCS superconductor, neglecting local fluctuations. The rough estimates based on the measured diffusion coefficients show that for typical SNSPD's $k_F l$ falls in the interval $1 \leqslant k_F l < 10$. Thus nanowire materials are on a metallic side of metal-insulator transition, and the use of the disordered superconductor model is at least qualitatively justified. While *a priori* justification of the model validity in view of the system being far from the asymptotic limit $k_F l \gg 1$ may be difficult, the convincing qualitative and quantitative agreement that we will demonstrate in this work provides strong *a posteriori* justification. The role of specific features of strong disorder beyond the validity of the model may be discussed on a qualitative level. For example, random local fluctuations of the order parameter, may significantly influence thermal diffusivity of quasiparticles through local Andreev reflections.

We start by discussing the density of states (DOS) in a superconductor carrying supercurrent. In the dirty limit the expression for DOS can be derived from the Usadel equation, which becomes [13]

$$\epsilon + i\Gamma \cos\theta = i\Delta \frac{\cos\theta}{\sin\theta}, \tag{1}$$

where ϵ is the energy, Δ is the order parameter, and θ is the pairing angle in the trigonometric representation of Green's functions. The depairing energy due to the supercurrent flow is $\Gamma = \hbar D/2(\nabla\Phi)^2 = 4\pi T_C (p_s \xi_0/\hbar)^2$, where $\nabla\Phi$ is the phase gradient, p_s is the condensate momentum, and $\xi_0 = \sqrt{\hbar D/2\pi T_C}$ is the coherence length for the disordered superconductor. More generally, we may write $\Gamma = \Gamma_0 + \hbar D/2(\nabla\Phi)^2$ adding the current independent component, Γ_0. The latter may be due to the presence of a magnetic field, spin-flip scattering, or introduced phenomenologically for a strongly disordered superconductor. The order parameter, the depairing energy, and the pairing angle θ depend on temperature, T, and the magnitude of the supercurrent. θ is also a function of ϵ. The dimensionless density of states in units of $2N(0)$, where $N(0)$ is the normal state DOS per spin at the Fermi level, is $\rho(\epsilon,\Gamma,\Delta) = \mathrm{Re}[\cos\theta(\epsilon/\Delta,\Gamma/\Delta)]$. Figure 1 shows DOS in a disordered current-carrying superconductor for a range of normalized pair-breaking energies. When $\Gamma/\Delta \neq 0$ the gap in the spectrum of elementary excitations differs from the order parameter. A change in supercurrent affects both the depairing energy Γ and the order parameter, Δ, as well as their ratio.

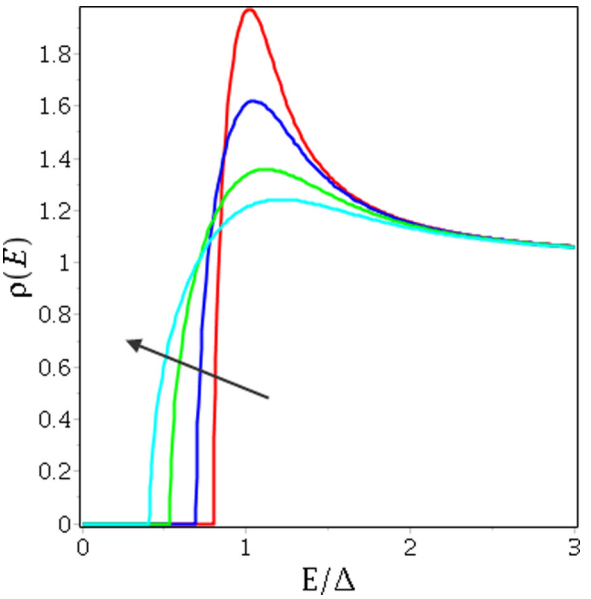

FIG. 1. (Color online) Normalized density of states in a disordered current-carrying superconductor for different depairing energies $\Gamma/\Delta = 0.05$ (red), 0.1 (blue), 0.2 (green), and 0.3 (cyan). The black arrow indicates the direction of increasing pair breaking energy.

Another implication of strong disorder is the enhanced electron-electron scattering leading to fast thermalisation. In typical NbN SNSPD wires, the inelastic scattering time, which may be attributed to electron-electron interaction, is $\tau_{ee} \sim 7$ ps [1]. This is considerably shorter than all other relevant times describing hotspot dynamics. Since NbN and WSi thin films have similar transport properties, we assumed that WSi films also have strong electron-electron scattering. In what follows we will use the concept of quasiequilibrium distribution, which may be characterized by a slowly varying temperature, both spatially and temporarily. The relaxing distribution of QPs in the current-carrying superconductor is a particularly interesting example. If the magnitude of the supercurrent is fixed, then with the temperature of excitations slowly changing, both the depairing energy and the order parameter must change accordingly, defining the QP relaxation path, which must be consistent with the constant magnitude of supercurrent.

The relation between current, order parameter, and temperature for a dirty superconductor can be found from Usadel equations. This can be done from the general solution of Kupriyanov and Lukichev [14] for a 1D nanowire numerically, or following Romijn *et al.* [15], who derived an approximate analytical result coinciding with the exact solution for the dirty limit $l << \xi_0$ (l is the electron elastic mean free path) and the arbitrary temperature interval within 1% accuracy. For consistency we must consider the case $\Gamma_0 = 0$, because both

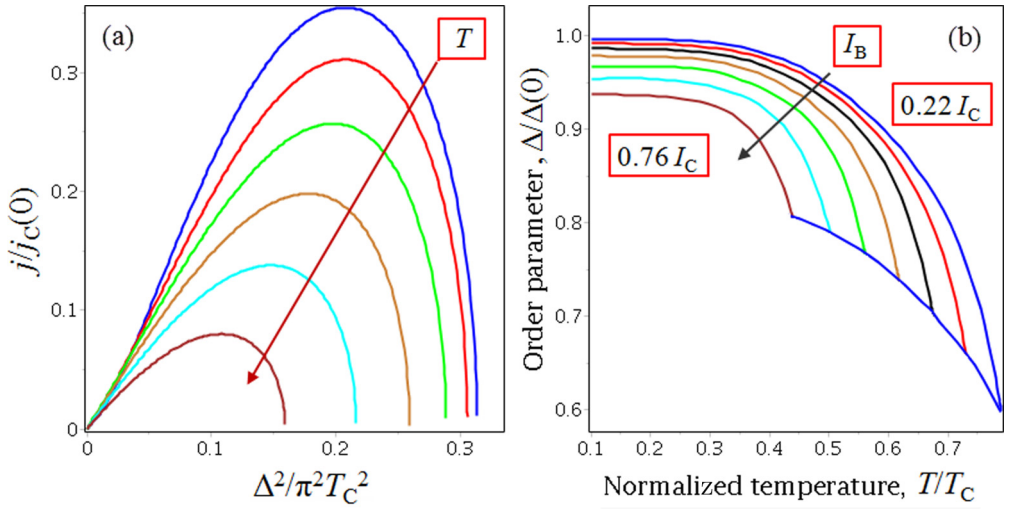

FIG. 2. (Color online) (a) Dependence of a current in a superconducting nanowire on square order parameter in the interval of temperatures from $0.3T_C$ to $0.8T_C$ with $0.1T_C$ increment from top to bottom. (b) Order parameter as a function of QP temperature in a dirty superconducting nanowire carrying a current. Arrow shows the direction of current increase from 0.22 to $0.76I_C$ with an increment of $0.09I_C$.

spin-flip scattering and magnetic field were disregarded in the derivation [14,15]. In strongly disordered thin superconducting nanowire films, the rounding off of the density of states that is seen in experiments [16,17] is attributed to extra depairing energy due to disorder rather than any specific pair-breaking mechanism. Correspondingly, when evaluating the density of states we will keep the parameter Γ_0 nonzero.

Below we will use the approach by Romijn *et al.* [15]. We have

$$\frac{j_B}{j_C(0)} = \frac{21\sqrt{3}\zeta(3)}{4\pi^{3/2}}\bar{T}\varphi^{1/2}\left[\sum_{n=0}^{\infty}\frac{\bar{\Delta}^2}{\bar{\Delta}^2+(2n+1)^2\bar{T}^2} - \frac{2}{\pi}\varphi\sum_{n=0}^{\infty}\frac{\bar{\Delta}^2(2n+1)^2\bar{T}^2}{(\bar{\Delta}^2+(2n+1)^2\bar{T}^2)^{5/2}}\right], \quad (2)$$

where

$$\varphi = \pi\left[\sum_{n=0}^{\infty}\left(\frac{\bar{T}}{\sqrt{\bar{\Delta}^2+(2n+1)^2\bar{T}^2}} - \frac{1}{2n+1}\right) - \frac{1}{2}\ln\bar{T}\right] \times\left[\sum_{n=0}^{\infty}\frac{(2n+1)^2\bar{T}^3}{(\bar{\Delta}^2+(2n+1)^2\bar{T}^2)^2}\right]^{-1}, \quad (3)$$

where j_B is bias current density. The normalization coefficient, $j_c(0)$, enters the Ginzburg-Landau expression for critical current density, $j_c = j_c(0)(1-T/T_c)^{3/2}$. Here $\bar{T} = T/T_C$ is temperature in units of T_C and $\bar{\Delta} = \Delta/\pi T_C$ is the order parameter in units πT_C. φ is a dimensionless (in units of critical temperature) part of the depairing energy associated with supercurrent [15], $\varphi = (\hbar D/2T_C)(\nabla\Phi)^2$.

Figure 2(a) shows the dependence of current on the square order parameter at different temperatures calculated using Eq. (2). Setting the current to a specific value in Eq. (2), we calculate the temperature dependence of the order parameter at that bias current. This is equivalent to intersecting the curves in Fig. 2(a) with horizontal lines (only the solution corresponding to higher order parameter is stable). This dependence is shown in Fig. 2(b). The temperature in Fig. 2(b) is in units of T_C, the order parameter is in units $\Delta(0)$ (which is its value at zero temperature and zero current), and the set of curves is for dimensionless bias current $I/I_c = 0.22, 0.31, 0.40, 0.49, 0.58, 0.67$, and 0.76 (increasing in the direction of the arrow). The temperature and the order parameter at the lower end of each curve are the critical temperature and the order parameter at the edge of the transition from superconducting to normal state at a particular current. Finally, Fig. 3(a) shows the calculated temperature at the critical (end) point, T_{CB}, for the set of relaxation curves in Fig. 2(a), Fig. 3(a) for the temperature, and Fig. 3(b) for the order parameter. The data in Figs. 3(a) and 3(b) if plotted as $\Delta_{C,I_B}/\Delta(0)$ vs T_{CB}/T_C will form the solid curve "supporting" the set of curves in Fig. 2(b) from the bottom.

Figure 4 introduces definitions which we will use in the paper. For illustration purposes we have chosen the top curve from Fig. 2(b), which corresponds to the relaxation path at bias current $I_B = 0.22I_C$. We will assume that in a disordered wire, the QP system comes to a quasiequilibrium at an elevated temperature, T, instantaneously due to intense electron-electron collisions. Subsequent relaxation in which excess energy is dissipated due to phonon emission and escape into a substrate is characterized by much slower rates. Therefore, at any instance of time the relaxation process is fully described by the varying temperature of the nonequilibrium electronic distribution. Phonons, that are emitted during the relaxation process, are assumed to escape from the film. This simplest version is the one-temperature model. The justification for this model is that the nanowire is very thin, typically only a few nanometers thick, so that phonons are likely to escape from the film before they are reabsorbed by QPs or scatter in anharmonic processes. A more sophisticated model would include phonon reabsorption and phonon-phonon interactions. For strong phonon-phonon interactions this more sophisticated model would evolve into the two-temperature model, where the phonon distribution is described as a quasiequilibrium Planck distribution with the transient phonon temperature $T_B < T_{ph}(t) < T(t)$ differing from both the bath and the QPs temperature and relaxing with the relaxing hotspot.

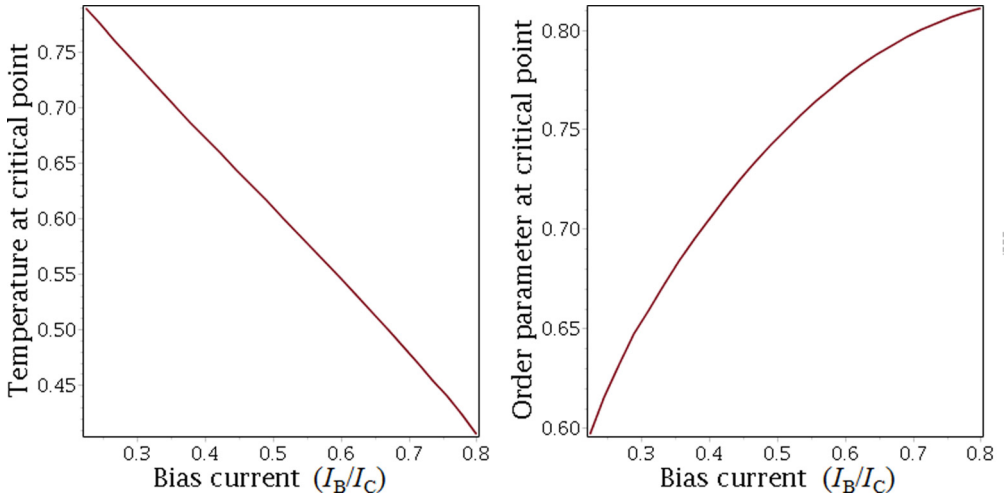

FIG. 3. (Color online) Dimensionless temperature, T_{CB}/T_C (a), and order parameter, $\Delta_{CB}/\Delta(0)$ (b), at critical (end) points of relaxation curves in Fig. 2(b) as a function of dimensionless bias current, I_B/I_C.

Before photon absorption at a site where a hotspot is created, a segment of the wire is at equilibrium (bath) temperature T_B. The corresponding state of this segment on the curve in Fig. 4 is shown by a solid circle. When a photon of energy E_λ is absorbed, part of its energy χE_λ is deposited into electronic system and the latter is heated to excitation temperature T_{ex}. The amount of energy, that is deposited into the QP system following the photon absorption event determines the initial state of the excited hotspot. There are the two scenarios where a large fraction of photon energy may be lost before the detection event occurs. On a shorter time scale $\tau_\varepsilon < t < L^2/D$, where τ_ε is the energy relaxation time, superconductivity may be broken in a small volume hotspot, with a lateral size which is less than the wire width, W, and hence does not significantly disrupt the supercurrent flow. Rapid thermalization inside the small size normal hotspot contributes to energy loss into the substrate due to escaping phonons. As a result, the expanding normal spot cools down and becomes superconducting before it reaches the edges. In the second case energy loss may occur during the primary energy down-conversion process. It is known that energy leakage from a thin film due to athermal phonons emitted in this process can be substantial [18–21], exceeding 60% in experiments with 40 nm thick W film on Si substrate [18]. For a few nanometer thick films in typical SNSPDs, even with disorder-enhanced phonon reabsorption, χ may be a few tenths due to escape of athermal phonons.

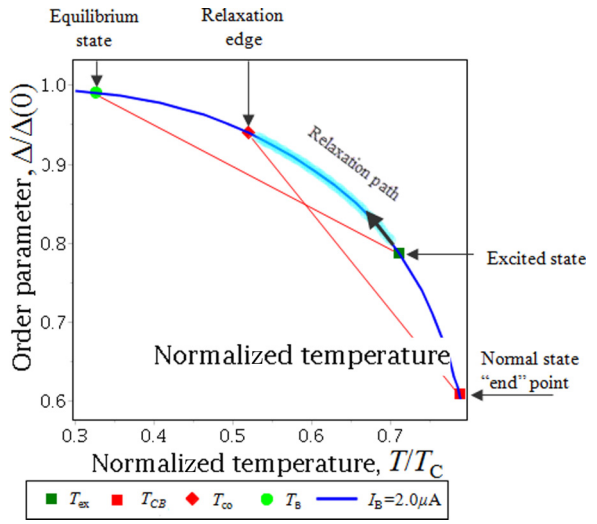

FIG. 4. (Color online) Different states of a nanowire and relaxation path of the hotspot.

Temperature T_{ex} characterizes the initial temperature of an excited hotspot at an internal quasiequilibrium after photon absorption. The hotspot starts cooling in a relaxation process which proceeds along the path indicated by an arrow in the direction of what we call the "relaxation edge." At any point of the relaxation process, the temperature and order parameter lie on the curve shown in Fig. 4, which marks the relaxation path of the superconducting nanowire in the Δ vs T plane. By definition, when the relaxing system of QPs cools down to the relaxation edge at cutoff temperature, T_{co}, absorption of another E_λ photon can heat the segment only up to T_{CB}, thus taking the segment exactly to the edge of superconductor to normal metal transition. This is indicated in Fig. 4 by a transition to the lower end ("end" point) of the relaxation curve. The question of whether vortices play a crucial role in the detection mechanism of SNSPDs has received great interest recently [5–7,22–24]. Vortex generation can be easily incorporated into our model by slightly modifying the end points of relaxation. However, whether or not vortex generation is important, its inclusion should not radically modify our description of hotspot dynamics. The cutoff temperature, T_{co}, is an important characteristic of the relaxing hotspot. Once the hotspot cools below T_{co}, the absorption of a second photon with overlapping hotspot will not trigger a superconductor-normal metal transition, and hence will not be observed in the experiment. Correspondingly, the time it takes for a hotspot to cool down from the excited state at T_{ex} to the relaxation edge state at T_{co} has a meaning of its relaxation time. Hotspot relaxation is nonexponential, depending on the positions of T_{ex} and T_{co} on a chosen relaxation curve.

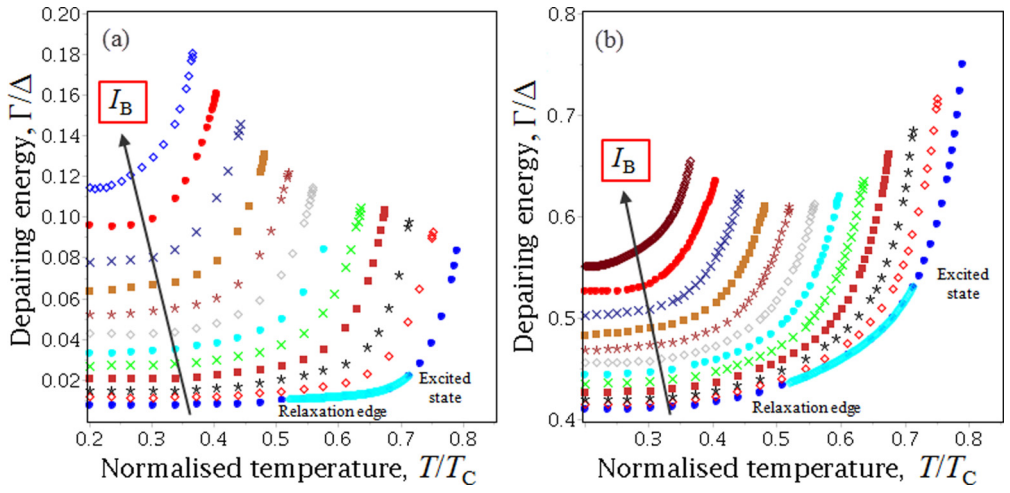

FIG. 5. (Color online) Ratio of pair-breaking energy to order parameter as a function of temperature in a dirty superconducting nanowire carrying a current. The current increases from 0.22 to $0.83I_C$ with an increment of $0.06I_C$ in the direction of the arrows: (a) $\Gamma_0 = 0$; (b) $\Gamma_0 = 0.2\Delta(0)$. Variations along the relaxation paths are shown for $I_B = 2\ \mu$A (continuous curves).

Variation of depairing energy along the relaxation path is given by $\Gamma = \Gamma_0 + \varphi T_C$, with φ changing according to (3). In Fig. 5 the temperature dependence of the ratio of depairing energy to order parameter is shown at different currents. These curves show relaxation paths at different currents in the Γ/Δ vs T plane. Along the vertical axis the dimensionless depairing energy in units of ambient order parameter is shown, and temperature is in units of T_C. The solid section of the lowest curve, corresponding to a bias current of $0.22I_c$, connects the excited state and the relaxation edge for the same conditions as in Fig. 4.

The expression for the QPs energy of a wire segment of volume V_{HS} has the form

$$E_{HS}(T,I_B) = 2N(0)V_{HS}\int_0^\infty d\epsilon\, \rho(\epsilon,\Gamma,\Delta)\frac{\epsilon}{\exp(\epsilon/T)+1}. \tag{4}$$

The dependence of E_{HS} on T and I_B comes through the Fermi distribution function and indirectly via corresponding functional dependencies of depairing energy Γ and order parameter Δ. Using the expression for $E_{HS}(T,I_B)$ we may determine the excitation temperature T_{ex} from the balance equation

$$E_{HS}(T_{ex},I_B) = E_{HS}(T_B,I_B) + \chi E_\lambda. \tag{5}$$

This balance reflects that after photon absorption the energy of a hotspot is the sum of the thermal energy at T_B and the deposited energy χE_λ bringing the temperature of the internally equilibrated electronic system to T_{ex}. Similarly, the balance for the relaxation edge is

$$E_{HS}(T_{CB},I_B) = E_{HS}(T_{co},I_B) + \chi E_\lambda \tag{6}$$

assuming that χ is independent of temperature, bias current, and photon wavelength. From (5) and (6) it follows that $T_{ex} = T_{ex}(I_B,T_B,E_\lambda)$ and $T_{co} = T_{co}(I_B,E_\lambda) > T_B$. Finally we define cutoff current I_{co} as the current above which the detector operates in the single-photon regime.

$$E_{HS}(T_{CB},I_{co}) = E_{HS}(T_B,I_{co}) + \chi E_\lambda. \tag{7}$$

The cutoff current is a function of bath temperature and wavelength, $I_{co} = I_{co}(T_B,\lambda)$.

Combining (5), (6), and (7) we arrive at the criteria determining the boundaries of the parameter space for the two-photon detection regime

$$T_B < T_{co}(I_B,E_\lambda) < T_{ex}(I_B,T_B,E_\lambda) < T_{CB}. \tag{8}$$

These criteria are easy to fulfill in WSi making this material especially suitable for studies of the two-photon detection regime.

III. DYNAMICS OF HOTSPOT RELAXATION IN SUPERCONDUCTING NANOWIRES

The physics underlying the formation of a normal region and its recovery in a superconducting nanowire following the absorption of a photon or other sources of energy deposition, for example due to impact with a particle or a molecule, is not fully understood. One of the most common descriptions [scenario (a) in Sec. I] assumes the initial formation of a normal (nonsuperconducting) region with a diameter less than the width of a nanowire. The supercurrent then is deflected, flowing around the normal spot so that its density on the sides increases above the critical current density, creating a normal region spanning across the wire. This scenario is realistic when the bias current is close to the critical current. However, the formation of the normal core hotspot after absorption of the first photon in a two-photon experiment at significantly lower bias currents will certainly not cause the current density on the sides of the normal core to exceed the critical value. In a recent experiment in NbN wires, the normal core hotspot model was found unlikely to be responsible for single photon detection of IR, visible, or UV photons [5].

In a two-photon experiment, a small normal core hotspot may potentially exist during the first few picoseconds after photon absorption. However, it cannot disrupt supercurrent flow because the bias current is small relative to the critical current of the wire. Because of the relatively small photon energy, the normal core, which cools as it expands, becomes

superconducting before it spans across the width of the nanowire. There is no photon detection event recorded after arrival of the first photon. In this situation we may disregard the evolution of the normal hotspot over the very short period of time before its conversion back to the superconducting state. Correspondingly, it does not matter whether the hotspot in two-photon experiments is initially normal. The nonequilibrium QP distribution can thus be characterized by a transient temperature below the critical value, T, and volume, V_{HS}, spanning across the nanowire. It is important that the second pulse only probes the state of relaxation of the nonequilibrium hotspot, providing information on whether the cutoff temperature has been reached. Therefore, the dynamics of a relaxing hotspot differ from the mechanisms leading to recovery of an SNSPD after a photodetection event. In a photodetection event, a normal region is created in the device, and the subsequent Joule heating [25] leads to much more energy being deposited into the device than the photon energy. The device recovers as it cools. Most of this recovery is via different processes than we discuss here. But once superconductivity is restored in the device, the remainder of the recovery should follow similar physics to those we outline here.

The dynamics of a nonequilibrium hotspot in a superconducting nanowire can be accurately described within the kinetic equation formalism [26–28]. The main simplifying assumptions of our model are (i) dirty superconductor limit and (ii) strong electron-electron scattering. The state of the phonon system is important for relaxation process. Therefore, we will consider the two limiting cases. In the first we assume weak anharmonic interactions, so that $\tau_{ph-ph} \gg \max\{\tau_{esc},\tau_{ph-e}\}$, where τ_{ph-ph} is the characteristic inelastic phonon-phonon relaxation time, τ_{esc} is the phonon escape time from the film, and τ_{ph-e} is the characteristic phonon reabsorption time by electronic system, either via breaking Cooper pairs or absorption by QPs. As a result, the nonequilibrium phonon distribution in the film is determined by phonon escape and reabsorption rates. For fast phonon escape, $\tau_{esc} \to 0$, and the distribution remains in equilibrium at the bath temperature. Thus this approach is the one-temperature (QPs) model. Within this model at any point with position x along the wire and time t we may characterize QPs system by the transient temperature $T(x,t)$. In the second limiting case, $\tau_{ph-ph} \ll \{\tau_{esc},\tau_{ph-e}\}$, and phonons are at quasiequilibrium characterized by their own transient temperature $T_B < T_{ph}(t) < T(t)$. This is the two-temperature model.

To discuss the dynamics of a cooling hotspot we write down the kinetic equation for the electron distribution function in a dirty superconductor. The distribution function can be written in the form [26]

$$\hat{f} = f\hat{1} + f_1\hat{\sigma}_z,$$

where $\hat{1}$ is identity matrix and $\hat{\sigma}_z$ is the Pauli matrix. For a strongly disordered nanowire with strong electron-electron scattering we may disregard f_1 and look for a solution of the form $f = 1 - 2n(\epsilon,T)$, modeling the electronic system as being at quasiequilibrium described by the Fermi function $n(\epsilon,T)$ with $T = T(x,t) > T_B$. Under this assumption, the kinetic equation can be written in the form

$$-D\frac{\partial}{\partial x}\left[\frac{\epsilon}{T}\frac{\partial n}{\partial \epsilon}\mathrm{Tr}(\hat{1} - \hat{g}^R\hat{g}^A)\frac{\partial T}{\partial x}\right] + \frac{\epsilon}{T}\frac{\partial n}{\partial \epsilon}\mathrm{Tr}(\hat{g}^R\hat{\sigma}_z - \hat{\sigma}_z\hat{g}^A)\frac{\partial T}{\partial t} + \frac{\partial n}{\partial \epsilon}\mathrm{Tr}\left(\frac{\partial \hat{\Delta}}{\partial t}(\hat{g}^R - \hat{g}^A)\right) = -2{I_1}^{ph}(n), \tag{9}$$

where

$$\hat{g}^{R(A)} = \begin{pmatrix} g^{R(A)} & f^{R(A)} \\ -f^{+R(A)} & -g^{R(A)} \end{pmatrix}, \quad \hat{\Delta} = \begin{pmatrix} 0 & -\Delta \\ \Delta^* & 0 \end{pmatrix}, \quad \hat{\sigma_z} = \begin{pmatrix} 1 & 0 \\ 0 & -1 \end{pmatrix}, \tag{10}$$

and ${I_1}^{ph}(n)$ is the collision integral describing all quasiparticle-phonon interactions in a superconductor, phonon emission, absorption, pair-breaking, and quasiparticle recombination. $g^{R(A)}$ and $f^{R(A)}$ are the quasiclassical retarded and advanced Green functions of a superconductor. Calculating traces we arrive at

$$-D\frac{\partial}{\partial x}\left\{\frac{\epsilon}{T}\frac{\partial n}{\partial \epsilon}[(g^R - g^A)^2 - (f^R - f^A)(f^{+R} - f^{+A})]\frac{\partial T}{\partial x}\right\} + \frac{2\epsilon}{T}\frac{\partial n}{\partial \epsilon}(g^R - g^A)\frac{\partial T}{\partial t}$$
$$+\frac{\partial n}{\partial \epsilon}\left[\frac{\partial \Delta}{\partial t}(f^{+R} - f^{+A}) + \frac{\partial \Delta^*}{\partial t}(f^R - f^A)\right] = -2{I_1}^{ph}(n). \tag{11}$$

The expression for the collision integral I_1^{ph} is

$$I_1^{ph} = -\frac{\pi\lambda_{ep}}{16\hbar(v_s p_F)^2}\int d\epsilon'(\epsilon - \epsilon')^2\left[2\left(g^R_{\epsilon'} - g^A_{\epsilon'}\right)\left(g^R_{\epsilon} - g^A_{\epsilon}\right) - \left(f^R_{\epsilon'} - f^A_{\epsilon'}\right)\left(f^{+R}_{\epsilon} - f^{+A}_{\epsilon}\right) - \left(f^R_{\epsilon} - f^A_{\epsilon}\right)\left(f^{+R}_{\epsilon'} - f^{+A}_{\epsilon'}\right)\right]$$
$$\times[(1 + 2N_{\epsilon'-\epsilon})(f_\epsilon - f_{\epsilon'}) - f_\epsilon f_{\epsilon'} + 1], \tag{12}$$

where λ_{ep} is the electron-phonon coupling constant, v_s is the mean sound velocity, and p_F is the Fermi momentum.

It is convenient to rewrite the kinetic equation using trigonometric parametrization of Green functions $\hat{g}^{R(A)} = \begin{pmatrix} \cos\theta^{R(A)} & e^{i\varphi}\sin\theta^{R(A)} \\ e^{-i\varphi}\sin\theta^{R(A)} & -\cos\theta^{R(A)} \end{pmatrix}$ arriving finally at

$$-D\frac{\partial}{\partial x}\left\{\frac{\epsilon}{T}\frac{\partial n}{\partial \epsilon}\left[\left(\mathrm{Re}\,\cos\theta_\epsilon^R\right)^2-\left(\mathrm{Im}\,\sin\theta_\epsilon^R\right)^2\right]\frac{\partial T}{\partial x}\right\}+\frac{\partial n}{\partial\epsilon}\left[\frac{\epsilon}{T}\mathrm{Re}\left(\cos\theta_\epsilon^R\right)-\frac{\partial|\Delta|}{\partial T}\mathrm{Im}\left(\sin\theta_\epsilon^R\right)\right]\frac{\partial T}{\partial t}$$
$$=\frac{1}{\tau_0}\int_0^\infty d\epsilon'\frac{(\epsilon+\epsilon')^2}{T_C^3}\left[\mathrm{Re}\left(\cos\theta_\epsilon^R\right)\mathrm{Re}\left(\cos\theta_{\epsilon'}^R\right)\mathrm{Im}\left(\sin\theta_\epsilon^R\right)\mathrm{Im}\left(\sin\theta_{\epsilon'}^R\right)\right][n_\epsilon n_{\epsilon'}-N_{\epsilon+\epsilon'}(1-n_\epsilon-n_{\epsilon'})]-{I_{1,a}}^{ph}(n)-{I_{1,e}}^{ph}(n), \tag{13}$$

where we introduced a characteristic relaxation time τ_0 according to $1/\tau_0=\lambda_{ep}T_C^3/\hbar(v_s p_F)^2$. The two collision integrals ${I_{1,a}}^{ph}(n)$ and ${I_{1,e}}^{ph}(n)$ describe quasiparticle scattering with absorption and emission of a phonon, respectively, while the explicitly written collision integral accounts for recombination. The "angle" θ^R defining the retarded Green function is the solution of the Usadel equation (1).

In what follows we consider the case $D\to 0$. This assumption is consistent with experimental data in WSi SNSPDs [4]. Neglecting spatial gradients, integrating the kinetic equation (13) over ϵ and taking into account conservation of quasiparticle numbers in phonon absorption and emission processes, i.e., $\int d\epsilon\, {I_{1,a,e}}^{ph}(n)=0$, we obtain

$$\frac{\partial\bar{T}}{\partial\bar{t}}=\bar{T}^4\int_0^\infty\int_0^\infty\frac{dz\,dz'(z+z')^2}{(e^z+1)(e^{z'}+1)}\left[1-\frac{N\left((z+z')\bar{T}/\bar{T}_B\right)}{N_0(z+z')}\right]$$
$$\times\left\{\varrho_1\left(\frac{z\bar{T}}{\alpha(\bar{T})},\beta(\bar{T})\right)\varrho_1\left(\frac{z'\bar{T}}{\alpha(\bar{T})},\beta(\bar{T})\right)+\varrho_2\left(\frac{z\bar{T}}{\alpha(\bar{T})},\beta(\bar{T})\right)\varrho_2\left(\frac{z'\bar{T}}{\alpha(\bar{T})},\beta(\bar{T})\right)\right\}$$
$$\times\left\{\int_0^\infty\frac{dz\,e^z}{(e^z+1)^2}\left[z\varrho_1\left(\frac{z\bar{T}}{\alpha(\bar{T})},\beta(\bar{T})\right)-\frac{\partial|\Delta|}{\partial T}\varrho_2\left(\frac{z\bar{T}}{\alpha(\bar{T})},\beta(\bar{T})\right)\right]\right\}^{-1}. \tag{14}$$

Here $N(\epsilon)$ is the nonequilibrium phonon distribution function, $N_0(z)=1/(e^z-1)$ is the Planck distribution function, and $\bar{t}$ is the normalized time in units of τ_0. We also use the notations $\varrho_1(\epsilon/\Delta(T),\Gamma(T)/\Delta(T))=\mathrm{Re}(\cos\theta_\epsilon^R)$ and $\varrho_2(\epsilon/\Delta(T),\Gamma(T)/\Delta(T))=\mathrm{Im}(\sin\theta_\epsilon^R)$ explicitly taking into account the dependence of the solution θ_ϵ^R of the Usadel equation (1) on $\epsilon/\Delta(T)$ and $\Gamma(T)/\Delta(T)$. Correspondingly we introduce functions α and β as $\alpha(\bar{T})=\Delta(T)/T_C$ and $\beta(\bar{T})=\Gamma(T)/\Delta(T)$ to impose a constraint on relaxation, which must proceed along the specific path as described above. Equation (14) is an integrodifferential equation describing recombination of quasiparticles within the hotspot. In its derivation we replaced $nn'(1+N)-N(1-n)(1-n')$ by $nn'(1-N/N_0(T))$, which is true for locally equilibrated QPs. The initial condition for Eq. (14) is given by (5). It can be solved numerically both to find the temperature evolution while the hotspot cools down and to determine the moment of time when the relaxation edge is reached so that $T(t_{HS})=T_{co}$.

To derive the expression for phonon distribution N, we write down the kinetic equation for phonons, neglecting terms with spatial gradients due to slow phonon diffusion:

$$\frac{\partial N}{\partial t}=-I_{esc}\{N\}-I_{ph-ph}\{N\}-I_{ph-e}\{N\}=-\frac{N-N_0(T_B)}{\tau_{esc}}-\frac{N-N_0(T_{ph})}{\tau_{ph-ph}}-\frac{N-N_0(T)}{\tau_{ph-e}}. \tag{15}$$

The escape time for a phonon from the film into the substrate for thicker film can be estimated using the familiar expression $\tau_{esc}=4d/\eta_t v_s$, where d is the film thickness and η_t is the phonon transmission coefficient into a substrate. For thin films with dominant phonon wavelengths exceeding the film thickness this expression cannot be justified and can only be used for rough estimates. In this situation the ratio $\gamma=\tau_{esc}/\tau_{ph-e}$ determining phonon bottleneck must be considered as a fitting parameter. The expression for phonon-electron time is

$$\frac{1}{\tau_{ph-e}(\epsilon,t)}=\frac{1}{\tau_B}\int_0^\infty\frac{d\epsilon'}{\Delta}[1-n(\epsilon',t)-n(\epsilon-\epsilon',t)]\left[\mathrm{Re}\left(\cos\theta_{\epsilon'}^R\right)\mathrm{Re}\left(\cos\theta_{\epsilon-\epsilon'}^R\right)+\mathrm{Im}\left(\sin\theta_{\epsilon'}^R\right)\mathrm{Im}\left(\sin\theta_{\epsilon-\epsilon'}^R\right)\right]$$
$$+\frac{2}{\tau_B}\int_0^\infty\frac{d\epsilon'}{\Delta}\left[n(\epsilon',t)-n(\epsilon+\epsilon',t)\right]\left[\mathrm{Re}\left(\cos\theta_{\epsilon'}^R\right)\mathrm{Re}\left(\cos\theta_{\epsilon+\epsilon'}^R\right)\mathrm{Im}\left(\sin\theta_{\epsilon'}^R\right)\mathrm{Im}\left(\sin\theta_{\epsilon+\epsilon'}^R\right)\right]=0 \tag{16}$$

and τ_B is characteristic pair-breaking time [29]. The first and second terms in (16) describe phonon reabsorption by condensate and electronic excitations, respectively. Because electron distribution is evolving on a slow time scale, τ_{ph-e} contains the corresponding time dependence. We use relaxation time approximation for the phonon-phonon collision integral and introduce τ_{ph-ph} as an extra parameter of the two-temperature model.

The time derivative in Eq. (15) can be disregarded because we are interested in the slow variation of phonon distribution relative to both phonon escape and reabsorption by electronic excitations. Neglecting this derivative and taking the limit $\tau_{ph-ph}\longrightarrow\infty$

we solve Eq. (15) and obtain for the one-temperature model

$$N(\epsilon,t)=\left[N_0(\epsilon,T_B)+N_0(\epsilon,T(t))\frac{\tau_{esc}}{\tau_{ph-e}(\epsilon,t)}\right]\left[1+\frac{\tau_{esc}}{\tau_{ph-e}(\epsilon,t)}\right]^{-1}. \tag{17}$$

For the two-temperature model taking $\tau_{ph-ph}\to 0$ we obtain

$$N(\epsilon,t)=N_0(\epsilon,T_{ph}). \tag{18}$$

In this case we need to determine phonon temperature, T_{ph}. The latter is to be found from the balance between the energy dissipated into a phonon system by QPs and the energy transferred by escaping phonons into a substrate. In the quasistationary conditions the rate of energy loss from QPs to phonons in electron-phonon interactions is equal to the energy gain by phonons in phonon-electron interactions Correspondingly we obtain

$$\begin{aligned}\sum_{\mathbf{k},j}\hbar\omega_{\mathbf{k},j}I_{esc}\{N\}&=\sum_{\mathbf{k},j}\hbar\omega_{\mathbf{k},j}I_{ph-e}\{N\}\int_0^\infty d\omega\,\omega^3\tau_{esc}^{-1}[N_0(\omega,T_{ph})-N_0(\omega,T_B)]\\&=\int_0^\infty d\omega\,\omega^3\tau_{ph-e}^{-1}(\omega,T)[N_0(\omega,T_{ph})-N_0(\omega,T)].\end{aligned} \tag{19}$$

A simple solution of (19) can be found by neglecting the dependence of the phonon's characteristic time on its energy and electron temperature, replacing $\tau_{ph-e}(\epsilon,T)$ by some average number, $\bar{\tau}_{ph-e}$. The solution is then

$$T_{ph}=\left[\frac{T_B^4}{1+\gamma}+\frac{\gamma T^4}{1+\gamma}\right]^{1/4}=\left[T_B^4+\frac{\gamma}{1+\gamma}\left(T^4-T_B^4\right)\right]^{1/4}=\left[T^4-\frac{1}{1+\gamma}\left(T^4-T_B^4\right)\right]^{1/4}. \tag{20}$$

As it follows from (20) phonon temperature lies in the interval $[T_B,T]$. We will consider γ as a constant, although this approximation is not entirely accurate, because γ slightly changes along the relaxation path. Substituting (17) instead of N into the expression (14) yields for the one temperature model

$$\begin{aligned}\frac{\partial\bar{T}}{\partial\bar{t}}=\bar{T}^4\int_0^\infty\int_0^\infty&\frac{dz\,dz'(z+z')^2}{(e^z+1)\left(e^{z'}+1\right)}\left[1+\frac{\tau_{esc}}{\tau_{ph-e}((z+z')\bar{T},\bar{t})}\right]^{-1}\left[1-\frac{N_0\left((z+z')\bar{T}/\bar{T}_b\right)}{N_0(z+z')}\right]\\&\times\left\{\varrho_1\left(\frac{z\bar{T}}{\alpha(\bar{T})},\beta(\bar{T})\right)\varrho_1\left(\frac{z'\bar{T}}{\alpha(\bar{T})},\beta(\bar{T})\right)+\varrho_2\left(\frac{z\bar{T}}{\alpha(\bar{T})},\beta(\bar{T})\right)\varrho_2\left(\frac{z'\bar{T}}{\alpha(\bar{T})},\beta(\bar{T})\right)\right\}\\&\times\left\{\int_0^\infty\frac{dz\,e^z}{(e^z+1)^2}\left[z\varrho_1\left(\frac{z\bar{T}}{\alpha(\bar{T})},\beta(\bar{T})\right)-\frac{\partial|\Delta|}{\partial T}\varrho_2\left(\frac{z\bar{T}}{\alpha(\bar{T})},\beta(\bar{T})\right)\right]\right\}^{-1}.\end{aligned} \tag{21}$$

The expression (21) contains the well-known phonon bottleneck factor $[1+\tau_{esc}/\tau_{ph-e}((z+z')\bar{T},\bar{t})]^{-1}$ accounting for the effect of phonon escape from the film relative to phonon reabsorption. In the two-temperature model, slow escape of phonons from the film also results in a progressively slowing recombination rate. This effect is seen as a substantial decrease of the term $[1-\frac{N_0((z+z')\bar{T}/\bar{T}_{ph})}{N_0(z+z')}]$ with $\gamma\to\infty$ because the temperature of slowly escaping phonons $T_{ph}\to T$.

IV. COMPARISON WITH EXPERIMENT

The full description of the experiment and the complete set of data is presented in our original work [4]. In the two photon experiment a photon count rate (*PCR*) as a function of delay time t_D was studied for a variety of different bias currents and bath temperatures. In our experiment we biased the superconducting nanowire single photon detector in a regime where it is sensitive to photon pairs. Therefore, the detector clicks only when two photons create two spatially overlapping hotspots. If the two hotspots are created at different times, then the second hotspot must be created before the first hotspot relaxes.

The experimentally observed Lorenzian line shapes of $P_{\text{click}}(t_D)$ curves can be derived within a model that accounts for spatial and temporal profiles of temperature inside the hotspot, and in particular its expansion due to out-diffusion. With a nonhomogeneous temperature distribution in the hotspot, the concept of cutoff temperature must be reexamined, because energy density is different in different parts of the hotspot. Correspondingly, breaking superconductivity in the part of the initial (pump) hotspot depends on the details of spatial overlap of hotspots created by the first and the second photons. This is a complicated situation to model. Within our current model, which neglects diffusion, the QP temperature is homogeneous throughout the hotspot, and the detector clicks as long as the two hotspots have nonzero spatial overlap. If temperature is homogeneous throughout the hotspot then the normalized photon count rate is $PCR=1/2L_{HS}\int_{-L_{HS}/2}^{L_{HS}/2}dx\,\Theta[T(t_D)-T_{co}]\Theta[L_{HS}-|x|]=\Theta[T(t_D)-T_{co}]$, where $\Theta(x)$ is the Heaviside function, that implies that PCR has a rectangular, not a Lorentzian, profile as a function of time delay t_D. The dependence of *PCR* on t_D can be correlated to the hotspot relaxation dynamics. Indeed, it drops by a factor 2 at $t=t_{HS}$ determined from $T(t_{HS})=T_{co}$, defining $\Theta(0)=1/2$. In our experiment,

t_{HS} was determined from the half width at half maximum (HWHM) of the $P_{\rm click}(t_D)$ curves. Thus the measured HWHM of the $P_{\rm click}(t_D)$ curve relative to a level of $P_{\rm click}(\infty)$ can be interpreted as the hotspot relaxation time. The rectangular shape of the theoretical *PCR* versus t_D curve is a consequence of our idealized model, which also assumes an unrealistic steplike shape of the *PCR* versus bias current curve. We anticipate that a model correctly accounting for the sigmoidal shape of *PCR* versus I_B observed in real devices would also predict bell-shaped *PCR* versus t_D curves that resemble the experimental data. In the near future, we plan to improve our model by accounting for the nonideal shapes of *PCR* as a function of both I_B and t_D, hopefully leading to a better understanding of detection mechanisms and hotspot dynamics.

The material parameters for tungsten silicide films depend on growth, stoichiometry, and annealing, and many of them are not known. If we take the mean sound velocity in W, $v_s = 3.2 \times 10^5$ cm/s, which is also close to the measured values for the transverse acoustic waves in tungsten silicide films [30], and the transmission coefficient for WSi/Si interface, $\eta_t \simeq 0.5$, we obtain for a rough estimate $\tau_{esc} \simeq 10.0$ ps. The pair-breaking time in WSi is also unknown. The range of variation of pair-breaking time in elemental superconductors with similar magnitudes of the order parameter is from 4.2 ps in Nb and 22 ps for Ta to 169 ps in In and 205 ps in Tl on the other end [29]. It is unlikely that $\gamma \gg 1$. According to Osofsky *et al*, [31] the strong increase in T_C in WSi alloy when Si content is increased occurs as a result of weakening in screening leading to a substantial enhancement of an attractive potential and corresponding increase of Eliashberg function. Using the McMillan empirical formula [32] for electron-phonon coupling constant $\tilde{\lambda}_{ep}$ from the experimentally determined transition temperature T_C, and Debye temperature, we estimate that $\tilde{\lambda}_{ep}^{WSi}/\tilde{\lambda}_{ep}^{W} \approx 2.0$ for a tungsten silicide alloy with $T_C = 4.5$ K. Calculation of Fermi surfaces of tungsten silicide alloys [33] reveals that for a tungsten-rich simple cubic W_3Si (i.e., a composition with high critical temperature) the density of states at the Fermi level is $N(0) \simeq 23.5 \times 10^{21}$ cm^{-3} eV^{-1}. In order to express the Eliashberg function of an alloy in terms of its electron-phonon coupling constant we also use the Debye model for the phonon spectrum. We finally arrive at the rough estimate $\tau_{ph-e}^{WSi} \simeq 2.7\tau_{ph-e}^{Ta} \approx 60$ ps and hence the expected interval $0.1 \leqslant \gamma \leqslant 1$. The one-temperature model is justified in the limit $\gamma \ll 1$ as seen from (20). Using the expression (20) for $\gamma \geqslant 1$ is an approximation assuming equilibration of phonons.

A. Hotspot relaxation depending on photon wavelength

The experimental data exhibit a strong dependence of hotspot relaxation on the wavelength of incident photons. In Fig. 6 we plot the excitation and cutoff temperatures of quasiparticles as a function of bias current for hotspot excitation by photons of different wavelengths. The vertical arrows close to the vertical dotted line, corresponding to a specific bias current, connect the excitation and cutoff temperatures. The lengths of these arrows indicate the lengths of relaxation paths for different photons. It is seen that the lengths of the relaxation paths are strong functions of photon wavelength and bias current.

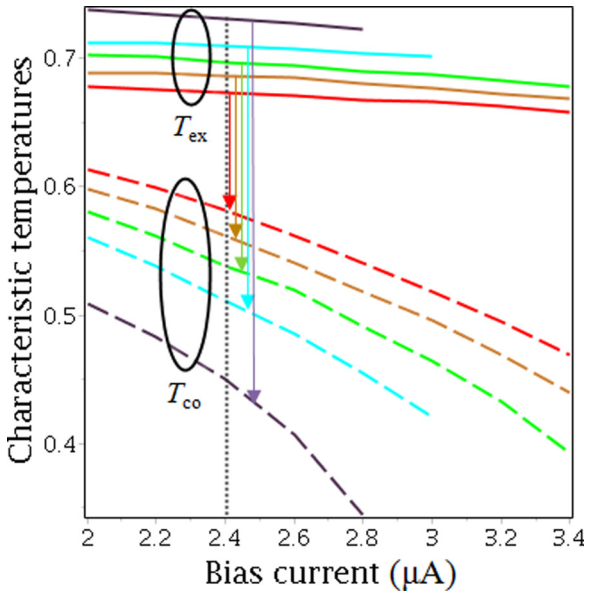

FIG. 6. (Color online) Hotspot excitation, T_{ex} (solid lines), and cutoff, T_{co} (dashed lines), temperatures as a function of bias current for photons of different wavelengths, $\lambda = 1200$, 1350, 1450, 1550, and 1650 nm (solid lines - from top to bottom, dashed lines - in the reversed order). Bath temperature is $T_B = 250$ mK.

The initial and final conditions for a relaxing hotspot are set by the initial excitation temperature, relaxation edge, and relaxation path. These are determined by the energy deposition parameter, δ, which we define as the ratio of the fraction of photon energy, that is deposited in the electronic system of the hotspot, to the unperturbed condensate energy within its volume, $\delta = \chi/2N(0)V_{HS}k_B^2T_C^2$. It is expressed in terms of a combination of three parameters, χ, $N(0)$, and V_{HS}. The density of states $N(0)$ can be independently evaluated, for example in electronic heat capacity measurements at low temperatures. This data however is not available. It can be roughly estimated using the Einstein relation and the measured diffusion coefficient. The diffusion coefficient in our WSi film is $D \approx 0.75$ cm^2/s as determined from the measured temperature derivative of the second critical field. The square resistance of our film is 476Ω. Thus $N(0) = 20.3 \times 10^{21}$ eV^{-1} cm^{-3}, which is consistent with the reported values for electronic heat capacity coefficient of tungsten [34] and is close to calculation [33]. Estimating the minimum hotspot area to be $W \times L_{HS} = 130 \times 100$ nm [4], where L_{HS} is the length of hotspot, we may finally relate δ to energy loss, χ, due to escaping athermal phonons. The latter may also be evaluated [21], providing further support for consistency of the model.

The energy deposition parameter δ determines the properties of the depleted superconductivity region in energy-current tomography experiments [5]. At first sight it is surprising that at as high photon energy as 3 eV in a single- and 8 eV in a multiphoton experiment, superconductivity in their NbN wire is not broken. Indeed, if energy E is homogeneously deposited into the electronic system within volume V_{HS}, the

temperature of this volume after thermalization is determined from the balance equation, $E = 2N(0)V_{HS}\int d\epsilon\,\epsilon\rho(\epsilon)n(\epsilon)$. At $T \to T_C$ and $\rho \to 1$ this determines the condition for the volume of hotspot, which is still in superconducting state, $V_{HS} \geqslant E(\pi^2/6N(0)k_B^2T_C^2)$. This estimate is correct for zero bias current. In current-carrying superconducting wire, the critical temperature depends on bias current, I_B, and is smaller than the zero-current critical temperature, $T_{CB} < T_C$. Correspondingly, the volume of the hotspot still in the superconducting state must exceed the estimate above. Taking the material parameters for NbN film from [35] we obtain $V_{HS} \geqslant 3.0 \times 10^{-4}\ \mu\,\mathrm{m}^3$. For 4 nm thick and 100 nm wide nanowire the length of hotspot, capable of accommodating the whole of photon energy, must reach $L \simeq 0.75\ \mu$m. The time it takes for the expanding QP cloud to fill this volume in 1D diffusion with $D = 0.4\ \mathrm{cm}^2/\mathrm{s}$ is $L^2/2D = 7.0$ ns. This time is more than two orders of magnitude larger than the relaxation time of optically induced hotspots in NbN superconducting nanowires (∼20 ps) [35–37]. The hotspot lateral size, L_{HS}, derived from the statistical weight of two photon detection events [4], is much smaller than ∼1 μm. Consequently, in order to have superconductivity suppressed, but not broken, only a fraction of photon energy must be deposited in the electronic system in WSi SNSPD. It can be estimated that in experiments [5] with $W = 220$ nm wide section of NbN wire in order to have depleted superconductivity in the hot spot of $\sim W^2$ area at bias currents $I_B \sim 0.5$–$0.6I_c$ and $E \simeq 3$–5 eV, the fraction of photon energy deposited into electronic excitations also must not exceed 10%–20%.

An example of the calculated evolution of temperature (in units T_C) in the hotspot along the relaxation path for $\lambda = 1200$ nm, $T_B = 250$ mK, and $I_B = 2.6\ \mu$A is shown in Fig. 7. Using our model, we quantitatively reproduced the wavelength dependence of t_{HS} with only three fitting parameters. The agreement between theory and experiment is good [4]. For all wavelengths we used the same set of three parameters, the

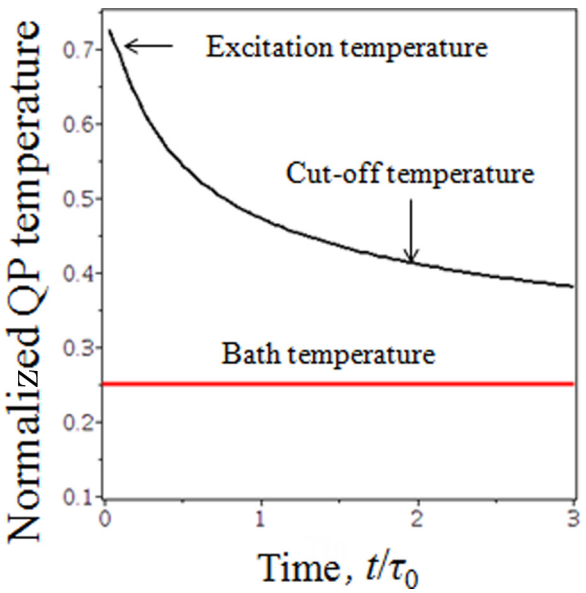

FIG. 7. (Color online) Temperature evolution in the relaxing hotspot.

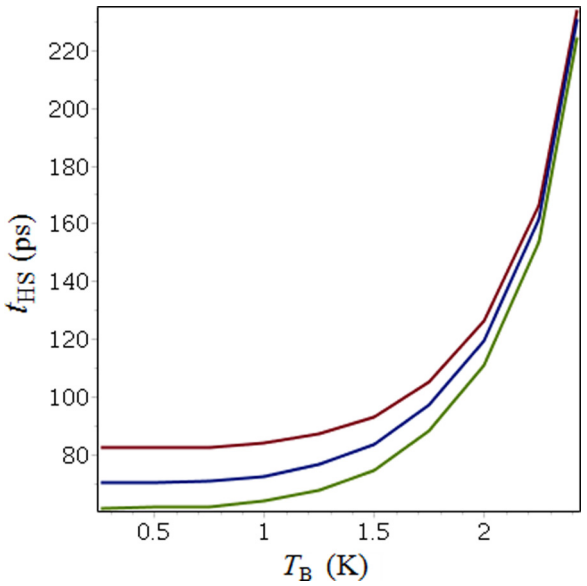

FIG. 8. (Color online) Hotspot lifetime as a function of bath temperature at fixed bias current $I_B = 2.0\ \mu$A for $\gamma = 0$ top curve, $\gamma = 0.3$ middle curve, and $\gamma = 3$ bottom curve.

energy deposition factor δ, the phonon bottleneck parameter γ, and τ_0. The two latter parameters in combination only fix the matching of the data along the vertical axis, and do not affect the shapes of the curves. To check the effect of different γ's we calculate t_{HS} as a function of temperature for a fixed current for different γ's. The simulated curves are shown in Fig. 8. It is seen from Fig. 8 that changing γ from 0 to 3 results in $\leqslant 15\%$ difference between the curves relative to $\gamma = 0.3$ over the whole interval. The variations of t_{HS} over the whole temperature range are 3.6, 3.3, and 2.8 for $\gamma = 3$, 0.3, 0, respectively. Thus not knowing the exact value of γ results in ∼15% uncertainty in determining τ_0. At the same time a strong (∼3) variation of t_{HS} over the whole range of temperatures seen in Fig. 8 is altered by no more than 15%. Thus the factor γ is not important in determining the shapes of the t_{HS} curves.

The interpretation of the strong increase in relaxation time with the increase of bias current is straightforward. Indeed, the main result of the model is to show that hotspot relaxation occurs due to self-recombination. The relaxing hotspot is strongly nonlinear. Nonlinearity is inevitable for the process of self-recombination. Moreover, a hotspot in an SNSPD is an exceptional example of a nonequilibrium nonlinear superconducting system, where all properties of the system (including spectrum of elementary excitations) continuously change along the relaxation path. A strong increase of relaxation time for larger bias currents is related to the increase of the difference between the initial temperature and the relaxation edge as seen from Fig. 7, where the slopes of the relaxation edge curves greatly exceed those for the initial temperature for all photon wavelengths. A dramatic slowdown (as seen in Fig. 7) occurs at the latest stages of the self-recombination process. The initial rate of self-recombination is so high for all bias currents that small

variations in the initial hotspot temperature have no significant impact on its relaxation time.

Complete relaxation depends on bath temperature. In the example in Fig. 7 bath temperature is 250 mK $\simeq 0.056T_C$ and complete relaxation will take time, which may exceed τ_0 by several orders of magnitude. At low bath temperatures, the bottleneck term in expression (14) is negligible, because in all situations the ratio $\frac{N((z+z')\bar{T}_b)}{N_0(z+z')}$ is very small and can be neglected. This is seen from Fig. 7 where T_{co} remains well above T_B. Under these circumstances the one-temperature model works very well.

B. Hotspot relaxation depending on bath temperature

When the bath temperature increases it may come closer and closer to the cutoff temperature defining the relaxation edge. The cutoff temperature itself does not depend on the bath temperature. In this situation the second term in the bottleneck expression, $\frac{N((z+z')\bar{T}/\bar{T}_B)}{N_0(z+z')}$, becomes more and more important when $T \to T_{co}$ affecting self-recombination rate and further slowing it down. Raising the bath temperature therefore results in an increase of t_{HS}. In this situation neglecting this term (as at low bath temperatures) can no longer be justified and a more realistic model of the phonon distribution function is necessary.

In Fig. 9 the black curve is T_{CB}, i.e., critical temperature at which the nanowire with current breaks normal. Above this curve we enter the single-photon regime, so that absorption of photon energy E_λ heats the section of nanowire above T_{CB} thus resulting in a photon count. The three lower curves give the initial temperature $T_{ex}(I_B)$ as a function of bias current for bath temperatures 2.0, 1.75, and 0.25 K from top to bottom. It is seen that the two-photon counting regime corresponds to bias currents not exceeding the value of cutoff current, I_{co}, determined by $T_{ex}(I_{co}) = T_C(I_{co})$. Thus with bath temperature

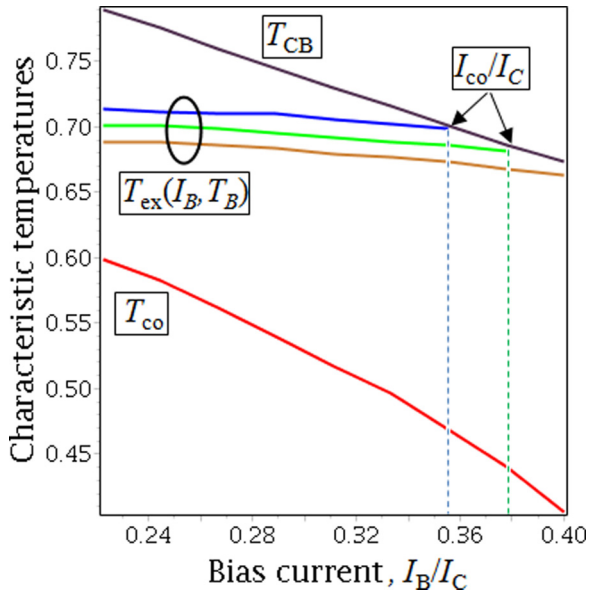

FIG. 9. (Color online) T_{CB}, $T_{ex}(I_B)$ for $T_B = 2.0$ K (blue), 1.75 K (green), and 0.25 K (orange) and T_{co} as a function of bias current for $\lambda = 1550$ nm.

increasing the two-photon regime can be realized at lower currents. This is exactly what was observed in the experiment.

Theoretical simulations of t_{HS} vs bias current at different temperatures of the bath, based on the developed model and the same set of three fitting parameters, δ, γ, and τ_0 as used for wavelength dependence, show good agreement with experiments at lower bath temperatures. However, it deteriorates at higher temperatures. Despite theory correctly predicting higher bath temperature behavior quantitatively the agreement is not as good as that at low T_B. This is a natural reflection of the importance of the detailed description of phonon distribution. The latter is likely to be better characterized by an elevated quasistationary temperature $T'_B > T_B$. One of the possible reasons for this is the relatively high laser power required to improve counting statistics in two-photon detection, resulting in a "dark" background temperature of the wire exceeding the bath temperature. In order to test the effect of elevated "bath temperature" we use as the fourth fitting parameter the bath temperature offset, ΔT, so that $T'_B = T_B + \Delta T$. The use of this extra fitting parameter results in excellent agreement with experiment [4].

C. Cutoff current fitting

In this subsection we discuss the cutoff current for single photon detection for the two reasons. The concept of cutoff current plays a central role in any physical model of an SNSPD. The main two families of curves from the two-photon detection experiments are (i) the functional dependencies of hotspot relaxation time versus bias current obtained for the range of photon wavelengths (1200–1650 nm) at a fixed bath temperature (250 mK) and (ii) the functional dependencies of hotspot relaxation time versus bias current obtained for the range of bath temperatures (0.25–2.5 K) at a fixed wavelength (1500 nm). As was demonstrated in our work [4], using the experimental data sets and plotting relaxation time t_{HS} as a function of bias current normalized to cutoff current results in all the curves exhibiting the same universal trend. It is also true for theoretical curves when they are replotted as a function of the normalized bias current. However, to prove that the four families of curves (the two for experiment, and the two for theory) follow the universal trend we must account for the differences between definitions of the cutoff currents in experiment and theory. Another reason is that experimental measurements of I_{co} versus bath temperature for a fixed photon wavelength and versus photon wavelength at a fixed bath temperature form a supplementary and independent set of data that can be analyzed to obtain further support for the introduction of temperature offset.

Figure 10 shows single photon system detection efficiency (a) and PCR (b) as a function of temperature and wavelength, respectively. Cutoff current was determined as the inflection point of each curve, following the procedure reported in the Supplemental Material of Ref. [38]. The theoretical definition in expression (7) refers to the onset of single photon sensitivity, corresponding to ideal signal detection efficiency SDE or PCR curves in the form of step functions. Assuming that both definitions result in the same functional dependencies, they can be compared after normalisation to the value of cutoff currents at $T_B = 0.25$ K for $I_{co}(T_B)$ and cutoff current at

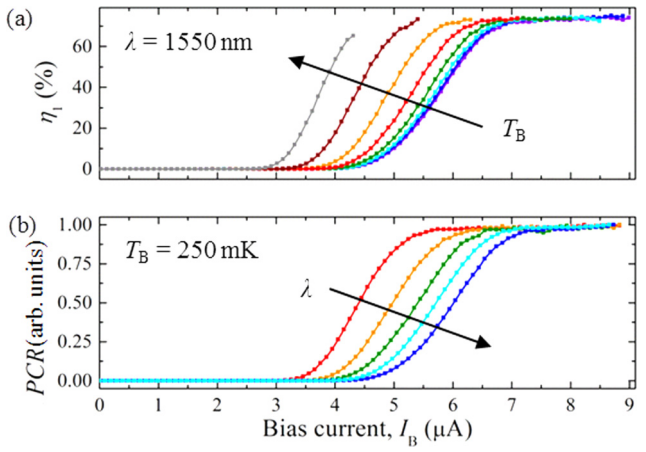

FIG. 10. (Color online) Single photon system detection efficiency (a) and PCR (b) as a function of temperature and wavelength, respectively.

$\lambda = 1200$ nm for $I_{co}(\lambda)$, respectively. The results of such a comparison are shown in Fig. 11. In Fig. 11(a) the experimental results (dotted line) for $I_{co}(T_B)$ differ from simulation, but practically coincide if the data are plotted as a function of $T_B' = T_B + 0.5$ K. Comparison of simulated and measured cutoff currents provides extra support to the argument that the effective phonon background temperature in the wire differs from the bath temperature. Temperature offset is not important in Fig. 11(b) as it was not important for low bath temperatures in Ref. [4].

The simulated cutoff current dependence on photon wavelength depicted in Fig. 11 can be compared to current-photon energy tomography experiments [5]. Linear dependence was observed in the measured combinations of bias current I_B and photon energy $E_\lambda = nhc/\lambda$, for which the detection probability equals 1% after the absorption of n photons over broad energy range 0.8–8 eV. The role of suppressed superconductivity was emphasized on the basis of current-carrying capacity of the wire being linearly dependent on the number of remaining Cooper pairs in the region of depleted superconductivity, and therefore on the photon energy. However, the legitimacy of the extrapolation of the observed linear dependence towards the lower photon energy limit E_λ could not be supported by any of the intuitive arguments. The nonlinearity of $I_B(E_\lambda)$ curve *a priori* cannot be excluded.

Theoretical simulation of cutoff current as a function of photon energy over the extended range beyond the experimental range of wavelengths in Fig. 11(b) is given in Fig. 12. As seen from this figure, linear extrapolation of the experimental data for $E_\lambda \to 0$ is not consistent with predictions of the kinetic model. The obvious reason is the strong change in the density of states, and therefore density of condensate, due to the increase of depairing energy Γ/Δ as bias current approaches the critical value. This results in the development of a substantially nonlinear response. Thus the reference current, I_0, obtained within the kinetic scenario as a linear intercept with the bias current axis, has no physical meaning. Such a reference current as seen from Fig. 12 is smaller than I_C. Moreover, the difference in temperature dependencies of "artificial" reference and critical currents is expected within

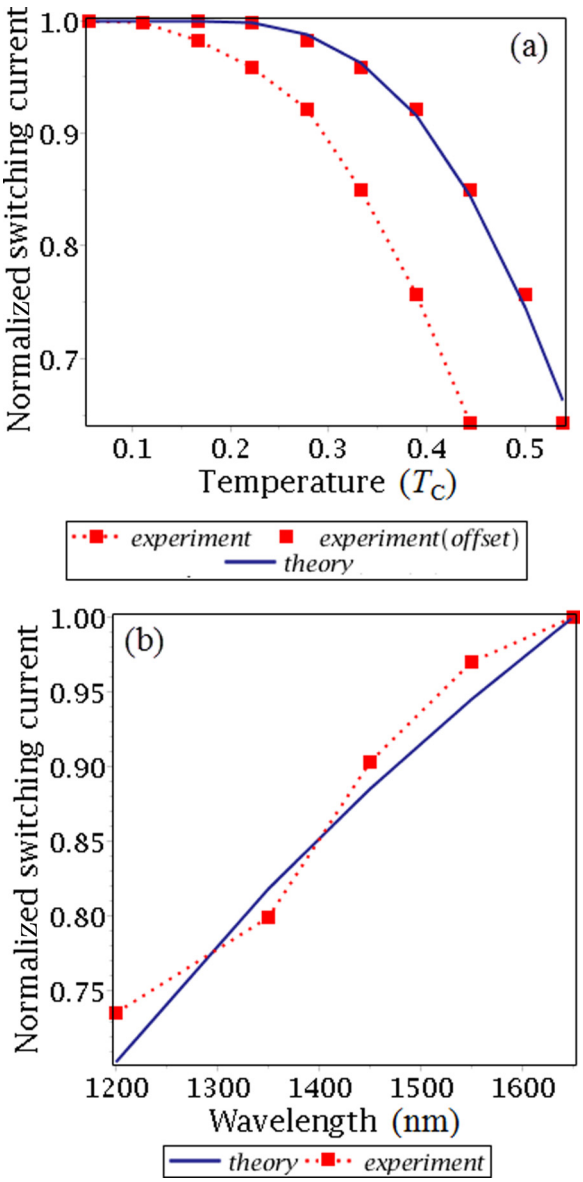

FIG. 11. (Color online) Normalized cutoff current as a function of bath temperature for $\lambda = 1550$ nm (a) and wavelength for $T_B = 250$ mK (b).

the detailed theory of hotspot dynamics. Linear bias current–photon energy dependence appears to be an approximation, which is justified for a limited photon energy range and bias currents outside the range $1 - I_B/I_C \ll 1$. Nonlinearity becomes more and more pronounced in the limit $E_\lambda \to 0$ and $I_B \to I_C$. Thus discrimination between mechanisms of single photon detection [5] requires more experimental and theoretical efforts.

So far in fitting theory to experiment we have used four parameters; energy deposition parameter δ, phonon bottleneck parameter γ, characteristic relaxation time, τ_0, and temperature offset, ΔT. We have shown that temperature offset is not important at low bath temperature; thus a good fit of $t_{HS}(I_B)$ for photons of different wavelengths was achieved with the use of only three fitting parameters. Fitting of $t_{HS}(I_B)$ for different bath temperature required the use of a fourth

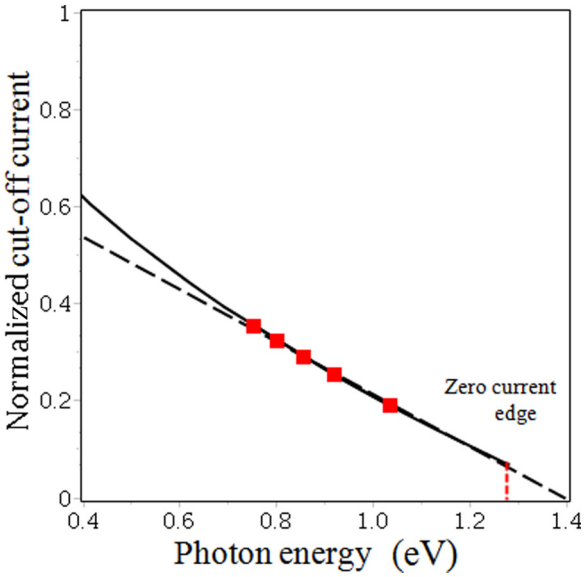

FIG. 12. (Color online) Cutoff current as a function of photon energy. Solid line: theory; solid boxes: experiment; dashed line: linear extrapolation.

parameter, ΔT. All simulations were done for the "intrinsic" material under the assumption of zero extra depairing energy, $\Gamma_0 = 0$. If extra depairing energy is of nonzero value, it can obviously affect the theoretical results. In order to understand the effect of finite Γ_0 we repeated all simulations for a large extra depairing energy. We chose $\Gamma_0 = 0.2\Delta(0)$. Figure 13 shows the comparison of simulations for $\Gamma_0 = 0$, solid curves, and $\Gamma_0 = 0.2\Delta(0)$, dash-dotted curves. It is seen from Fig. 13 that the sets of dash-dot curves describing the situation with extra depairing energy closely fits the set of solid curves for $\Gamma_0 = 0$. To achieve this we changed only two parameters—τ_0 by a factor of 0.75 relative to the case $\Gamma_0 = 0$, and temperature offset $\Delta T = 250$ mK compared to 500 mK for $\Gamma_0 = 0$. It is not surprising that with an extra depairing energy due to disorder a good fit is provided with the reduced temperature offset, keeping the overall depairing intensity similar for both cases. An extra depairing energy also induces shifts of excitation and cutoff temperatures, T_{ex} and T_{co}, resulting in appropriate adjustment in time scale, controlled by the value of the parameter τ_0.

Summarizing, variation of parameters γ, τ_0, Γ_0 over a broad phase space do affect the dynamics of a relaxing hotspot. However, the role of these parameters is largely in determining the time scale for the hotspot relaxation. The most profound effect is connected with the energy deposition parameter, δ, which directly determines the dynamical path and causes the hotspot relaxation time to vary by more than one order of magnitude.

D. Diffusion enigma

Our theoretical model explains our experimental data completely ignoring QP diffusion. In fact, the model was developed under the evidence drawn from the data that diffusion effects are not important, at least over time scales of the order of one nanosecond. This behavior presents an enigma, which deserves

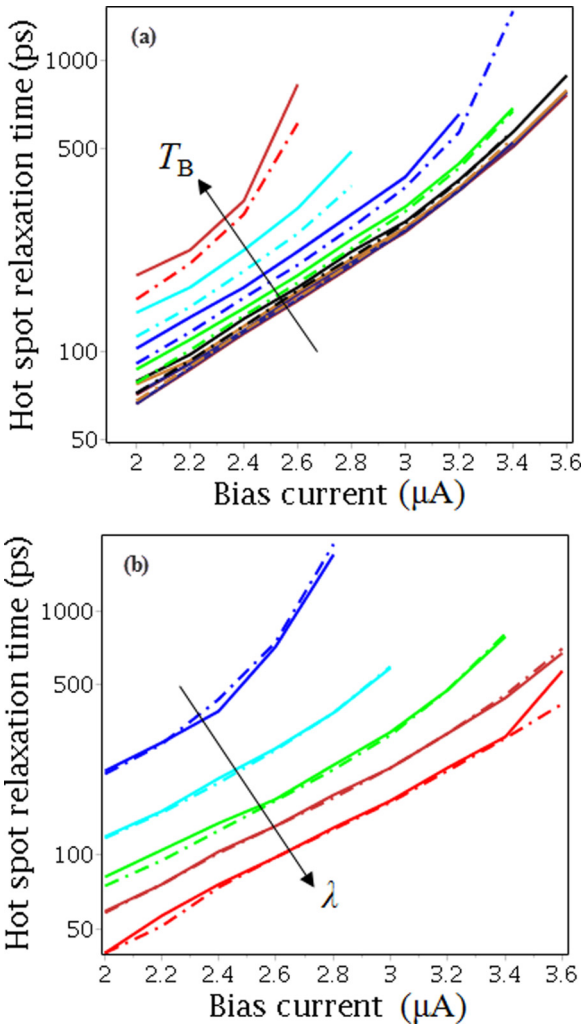

FIG. 13. (Color online) Hotspot relaxation time, t_{HS}, dependence on depairing energy Γ_0. (a) t_{HS} as a function of bias current for different bath temperatures from 0.25 to 2.0 K with an increment 0.25 K. An arrow indicates increasing bath temperature. Solid curves: $\Gamma_0 = 0$, $\delta = 325\,\text{meV}^{-1}$, $\gamma = 0.3$, $\tau_0 = 496$ ps, and $\Delta T = 500$ mK; dash-dot curves: $\Gamma_0 = 0.2\Delta(0)$, $\delta = 325\,\text{meV}^{-1}$, $\gamma = 0.3$, $\tau_0 = 375$ ps, and $\Delta T = 250$ mK. (b) t_{HS} as a function of bias current for different wavelengths: 1200, 1350, 1450, 1550, and 1650 nm; $T_B = 250$ mK. An arrow indicates increasing wavelength. Solid curves: $\Gamma_0 = 0$, $\gamma = 0.3$, $\tau_0 = 439$ ps, and $\delta = 325\,\text{meV}^{-1}$; dash-dot curves: $\Gamma_0 = 0.2\Delta(0)$, $\gamma = 0.3$, $\tau_0 = 330$ ps, and $\delta = 325\,\text{meV}^{-1}$.

special discussion. While experiment strongly indicates that diffusion effects surprisingly contribute a little to the hotspot relaxation this on its own is not an evidence of model limitations originating from finite values of the parameter $k_F l$. In this section, we discuss possible physical explanations for this behavior within the framework of our model.

The simplest estimate can be arrived at assuming constant thermal diffusivity of QPs; hence using a linear heat diffusion model. If at $t = 0$ the hotspot occupies the volume $\sim W^2 d$ and its temperature is T_{ex}, then due to 1D diffusion and expansion of hotspot volume it rapidly decreases, so that at $t = 0.2W^2/\tilde{D}$ and $t = 0.4W^2/\tilde{D}$ its maximum is at $\simeq 0.57$ and 0.42 T_{ex}, respectively. Here $\tilde{D}$ is the thermal diffusivity coefficient.

Assuming $\tilde{D} \sim 0.5D$, which is a reasonable estimate for $T \geqslant T_{co}$, we evaluate $0.2W^2/\tilde{D} \sim 90$ ps. If we take for example $\lambda = 1550$ nm and $I_B = 3.4$ μA, then $T_{co}/T_C = 0.44$. Thus, after $\sim$180 ps the maximum temperature in the center of the hotspot would be below the relaxation edge T_{co}, which would result in the full recovery of the hotspot. Even the shortest relaxation time at $I_B = 3.44$ μA, which was measured at the lowest bath temperature $T_B = 0.25$ K and is ≈ 500 ps, is considerably longer. This means that linear diffusion alone, without any self-recombination, would be capable of rapid cooling of the hotspot. Moreover, if diffusion dominates, the dependence $t_{HS}(T_B)$ must be absent, because in all situations $T_{co} > T_B$, and neither thermal diffusivity, $\tilde{D}$, nor cutoff temperature, T_{co}, depend on bath temperature. At the lowest bias currents, diffusion expansion predictions for cooling of the hotspot below the cutoff temperature are comparable to the measured relaxation time. However, the observed strong dependence of hotspot dynamics on bath temperature contradicts the predictions of the linear thermal diffusion model and thus rules it out from playing a significant role.

In photon detection experiments the order parameter is suppressed inside the hotspot. Some of the excited QPs will be trapped because of Andreev reflections at the boundaries. It is seen from Figs. 2(b), 3, and 8 that the suppression of the order parameter close to T_{co} relative to its zero temperature value is not strong, being in the range of 10%–15% for small bias currents and decreasing to approximately 5% for higher bias currents. Trapping of QPs slows down the overall diffusion. However, because of relatively high cutoff temperatures (in the range 0.4–0.6 T_C) the fraction of QPs experiencing Andreev reflection is not large, and the majority of QPs having energies above the edge of the gap outside the hotspot can freely diffuse out of the hotspot. Therefore, within the dirty superconductor model, which we used in this paper, and the linear expansion model this diffusion enigma cannot be fully resolved.

The factors that are likely to be important, either on their own or acting together, are strong disorder and nonlinear character of diffusion. There are indications of a high density of subgap states in strongly disordered superconductors near the metal-insulator transition [16]. Observations in strongly disordered TiN and NbTiN films were shown to be consistent with a model using strong pair breaking, dependent on the level of disorder. While pair-breaking energy results in a non-BCS density of states, this approach does not describe any changes in transport properties of QPs, which are necessary to address the diffusion problem; thus pair breaking cannot resolve this diffusion problem. Near the superconductor-insulator transition, a strongly fluctuating local order parameter [10] may be the missing link which is responsible for the dramatic change in transport. This may be due to hopping of QPs in the subgap region, or Andreev reflections from strong, random fluctuations in the local order parameter (random Andreev reflections) greatly reducing QP diffusivity and trapping them within the stable volume of the hotspot.

Finally, it turns out that for a typical hotspot the linear heat transport model itself cannot be justified. Indeed, in the divergence term in Eq. (13) the effective diffusion coefficient itself is a strong function of coordinate through the spatial dependencies of both the temperature and the order parameter. After differentiation there appear the terms proportional to $\partial^2 T/\partial x^2$ and $1/T(\partial T/\partial x)^2$ with coefficients depending on T and Δ. The term with the first derivative is zero at the center of the hotspot. Away from the center it greatly increases and has opposite sign to the term with the second derivative, thus weakening its contribution, which makes it appear that diffusivity in the center of the hotspot is suppressed. Nonlinearity becomes especially strong close to the edges of the hotspot, where it must influence both the spatial and temporal profiles of the temperature and the order parameter.

The nonlinear diffusion problem is mathematically very complicated. A simplified nonlinear thermal diffusion equation can be derived from Eq. (13) under a local approximation for Green functions or from the Larkin and Ovchinnikov kinetic equation [27]. Numerical solution of this problem confirms the effect of a slowdown of thermal expansion of the hotspot, so that the nonlinearity in thermal transport can account for the lesser role of diffusion in a relaxing hotspot. Despite the experimental evidence of the dominant role of self-recombination in relaxation of the hotspot, QP diffusion is nonetheless important. Even if relatively slow, it inevitably results in a slight spatial expansion of the hotspot and hence the spatial profile of the temperature. The most important variations for the two-photon experiment are those near the cutoff temperature. Depending on the spatial overlap of the two photon pulses the second photon's ability to cause a click for a fixed time delay is determined by whether the local temperature, $T(x,t)$, in the profile created by the two photons is larger or smaller than T_{co}. With time delay t_D increasing, the overlap area where $T(x,t) \geqslant T_{co}$ shrinks. Therefore, the shape of $t_{HS}(t_D)$ curves is likely to be directly linked to diffusive properties. The numerical analysis of nonlinear diffusion in hotspots is therefore an important problem and will be published elsewhere.

E. Two-photon detection in NbN SNSPD

The first two-photon detection experiments in NbN SNSPDs [1,36,37] revealed the hotspot relaxation time $t_{HS} \sim 20$ ps, which is a factor of 4 shorter than the shortest relaxation time that was measured in our WSi SNSPD [4]. Furthermore, t_{HS} was measured at a single [37] or very limited range of bias currents (0.48 to $0.55I_C$) [36], at a higher bias currents relative to the critical current than in WSi. In this range, according to predictions of our model, t_{HS} must rapidly increase with the current, so the detection of such a short time might look surprising. An interesting question is whether this is an indication of different hotspot dynamics in NbN, or if it is due to a significant difference in material properties, which was not well understood and not predicted.

In this situation it becomes worthwhile to analyze the results [36,37] applying our model. We first note that the energy deposition factor δ for NbN is likely to be smaller than in WSi. Comparing NbN to WSi we see that the mean value for N(0) of typical NbN SNSPD thin film is close to what we used for WSi. Diffusion coefficients in both materials are also close, and it is reasonable to assume the same rate of establishing local equilibrium in the hotspots in both materials. Thus, the diffusing clouds of nonequilibrium QPs fill nearly the same volumes in nanowires with the same width and thickness for both materials. The energy loss factor χ for WSi was estimated

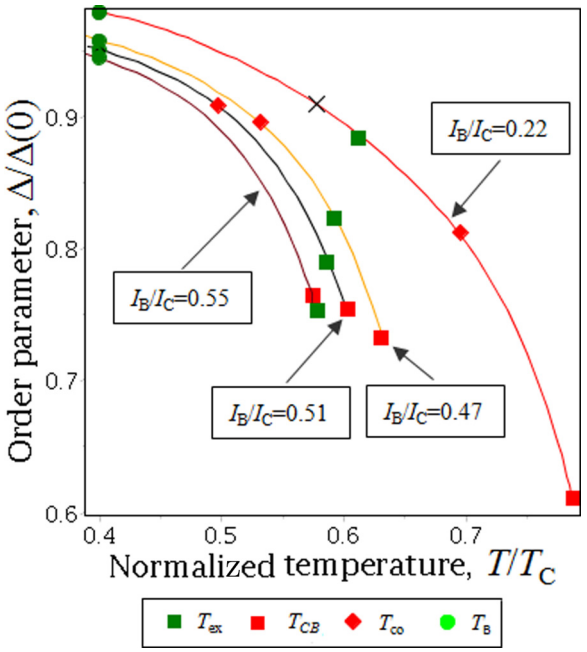

FIG. 14. (Color online) Hotspot relaxation paths for NbN nanowires at different currents.

from the best fit value of δ. In the absence of the appropriate data on two-photon detection in NbN, we cannot establish the best fit δ for the SNSPDs in Refs. [36,37]. Instead we may exploit some indirect data. The strongest material dependence comes through the inverse proportionality of δ to a square of the critical temperature; this alone is responsible for a factor $\sim$5 reduction. On the other hand, in the experiment [37] on NbN SNSPD on sapphire, a rough estimate of phonon escape time from the wire indicates a smaller athermal phonon loss, and correspondingly, a bigger fraction χ. In an experiment of Il'in *et al.* [39] the phonon bottleneck parameter was found to be $\gamma = 0.6$, twice the value that we used for WSi SNSPD (which is better acoustically matched to the Si substrate). Taking the ratio $\chi_{NbN}/\chi_{WSi} \sim 2$ and $T_C = 10$ K for NbN we arrive at $\delta \approx 129\,\mathrm{meV}^{-1}$. The smaller value of energy deposition factor means that even using more energetic photons [36,37], the biasing of an SNSPD at a considerably higher currents is required in NbN.

Like we did for WSi [see Fig. 2(b)], we calculated the relaxation paths for a NbN SNSPD operating in the two-photon regime at different bias currents. Figure 14 shows hotspot relaxation paths for bias currents of 0.22, 0.47, 0.51, and 0.55 of I_C. The bath temperature in the experiments was 4 K. As is seen for the lowest bias current $T_{ex} < T_{co}$. Even with ideal temporal and spatial overlap of hotspots the absorption of two photons will not result in a click, because the deposited energy is not sufficient for breaking superconductivity. In order for a click to occur for this bias current, the bath temperature must exceed the abscissa of the diagonal cross on the relaxation path. It is clear that the bias currents are limited on low side, i.e., the bias current must be sufficiently large so that $T_{ex} > T_{co}$. T_{ex} and T_{co} in Fig. 14 were calculated for $\delta = 129\,\mathrm{meV}^{-1}$. At the highest bias current $I_B/I_C = 0.55$, the SNSPD operates in the single-photon regime, because $T_{ex} > T_{CB}$. Thus to operate in the two-photon detection regime, the NbN SNSPD must be biased at $I_B/I_C < 0.55$. Comparing the relaxation paths at the two intermediate currents $I_B/I_C = 0.51$ and 0.47 we see that the length of relaxation path (distance from T_{ex} to T_{co}) rapidly decreases with only a small ($\sim$10%) decrease in bias current from 0.51 to 0.47 of I_C. This results in substantial shortening of t_{HS}, similar to our results for the WSi SNSPD. Calculating T_e transients for both curves, we find that t_{HS} at $I_B = 0.55 I_C$ is a factor of 1.9 shorter than t_{HS} at $I_B = 0.47 I_C$. Finally, fitting $t_{HS} = 20$ ps requires $\tau_0|_{NbN} \simeq 52$ ps. According to Kaplan [29] we have $\tau_0^{-1} \sim T_C^3$. Thus, assuming a similar electron-phonon coupling constant for both materials, we expect τ_0 in NbN to scale down by a factor of $\simeq$10 yielding the number close to 50 ps, which is consistent with the estimate above. Although in the absence of detailed experimental data for NbN this estimate cannot serve as proof of the same hotspot dynamics, nonetheless it is reassuring for its consistency with the model.

V. SUMMARY

In summary we developed a theoretical model of relaxation of the hotspots in superconducting current-carrying nanowires. We have shown that in tungsten silicide SNSPDs the hotspot generated by a photon below the threshold for single-photon detection relaxes in a self-recombination of nonequilibrium QPs. Strong dependencies of hotspot relaxation time on bias current, bath temperature, and photon wavelength are explained by specific dynamics of the hotspot, and are dominated by self-recombination, rather than diffusive expansion. The model satisfactorily explains all major experimental results. The reasons for the greatly suppressed role of quasiparticle diffusion are likely to be related to strongly nonlinear heat transport in a disordered superconducting nanowire close to a metal-insulator transition.

ACKNOWLEDGMENTS

A.G.K. and C.L. gratefully acknowledge financial support from the Engineering and Physical Sciences Research Council. Part of the research was carried out at the Jet Propulsion Laboratory, California Institute of Technology, under a contract with the National Aeronautics and Space Administration.

[1] A. D. Semenov, G. N. Gol'tsman, and A. A. Korneev, Physica C **351**, 349 (2001).
[2] A. Semenov, A. Engel, H.-W. Hübers *et al.*, Eur. Phys. J. B **47**, 495 (2005).
[3] J. K. W. Yang, A. J. Kerman, E. A. Dauler *et al.*, IEEE Trans. Appl. Supercond. **17**, 581 (2007).
[4] F. Marsili, M. J. Stevens, and A. Kozorezov *et al.*, arXiv:1506.03129.

[5] J. J. Renema, R. Gaudio, Q. Wanget *et al.*, Phys. Rev. Lett. **112**, 117604 (2014).
[6] L. N. Bulaevskii, M. J. Graf, C. D. Batista, and V. G. Kogan, Phys. Rev. B **83**, 144526 (2011).
[7] L. N. Bulaevskii, M. J. Graf, and V. G. Kogan, Phys. Rev. B **85**, 014505 (2012).
[8] A. Gurevich and V. M. Vinokur, Phys. Rev. Lett. **100**, 227007 (2008).
[9] A. Gurevich and V. M. Vinokur, Phys. Rev. B **86**, 026501 (2012).
[10] B. Sacépé, T. Dubouchet, C. Chapelier *et al.*, Nat. Phys. **7**, 239 (2011).
[11] D. Sherman, G. Kopnov, D. Shahar, and A. Frydman, Phys. Rev. Lett. **108**, 177006 (2012).
[12] B. Sacépé, C. Chapelier, T. I. Baturina, V. M. Vinokur, M. R. Baklanov, and M. Sanquer Phys. Rev. Lett. **101**, 157006 (2008).
[13] A. Anthore, H. Pothier, and D. Esteve, Phys. Rev. Lett. **90**, 127001 (2003).
[14] M. Yu. Kupriyanov and V. F. Lukichev, Fiz. Nizk. Temp. **6**, 445 (1980) [Sov. J. Low Temp. Phys. **6**, 210 (1980)].
[15] J. Romijn, T. M. Klapwijk, M. J. Renne, and J. E. Mooij, Phys. Rev. B **26**, 3648 (1982).
[16] E. F. C. Driessen, P. C. J. J. Coumou, R. R. Tromp, P. J.deVisser, and T. M. Klapwijk, Phys. Rev. Lett. **109**, 107003 (2012).
[17] P. C. J. J. Coumou, E. F. C. Driessen, J. Bueno, C. Chapelier, and T. M. Klapwijk, Phys. Rev. B **88**, 180505 (2013).
[18] B. Cabrera, R. M. Clarke, P. Colling *et al.*, Appl. Phys. Lett. **73**, 735 (1998).
[19] D. D. E. Martin, P. Verhoeve, A. Peacock *et al.*, Appl. Phys. Lett. **88**, 123510 (2006).
[20] A. E. Lita, A. J. Miller, and S. Nam, J. Low Temp. Phys. **151**, 125 (2008).
[21] A. G. Kozorezov, C. J. Lambert, S. R. Bandler, M. A. Balvin, S. E. Busch, P. N. Nagler, J.-P. Porst, S. J. Smith, T. R. Stevenson, and J. E. Sadleir, Phys. Rev. B **87**, 104504 (2013).
[22] D. Yu. Vodolazov, Phys. Rev. B **90**, 054515 (2014).
[23] A. N. Zotova and D. Yu. Vodolazov, Supercond. Sci. Technol. **27**, 125001 (2014).
[24] A. Engel, J. Lonsky, X. Zhang, and A. Schilling, IEEE Trans. Appl. Supercond. **25**, 2200407 (2015).
[25] A. J. Kerman, J. K. W. Yang, R. J. Molnar, E. A. Dauler, and K. K. Berggren, Phys. Rev. B **79**, 100509 (2009).
[26] A. I. Larkin and Yu. N. Ovchinnikov, in *Nonequilibrium Superconductivity*, edited by D. N. Langenberg and A. I. Larkin (Elsevier Science Publishers B. V., Amsterdam, 1986).
[27] A. I. Larkin and Yu. N. Ovchinnikov, Sov. Phys. JETP **46**, 155 (1977).
[28] N. B. Kopnin, *Theory of Nonequilibrium Superconductivity* (Clarendon Press, Oxford, 2001).
[29] S. B. Kaplan *et al.*, Phys. Rev. B **14**, 4854 (1976).
[30] G. M. Crean, A. Golansky, and J. C. Oberlin, Appl. Phys. Lett. **50**, 74 (1987).
[31] M. S. Osofsky, R. J. Soulen, Jr., J. H. Claassen, G. Trotter, H. Kim, and J. S. Horwitz, Phys. Rev. Lett. **87**, 197004 (2001).
[32] W. L. McMillan, Phys. Rev. **167**, 331 (1968).
[33] S. Itoh, J. Phys.: Condens. Matter **2**, 3747 (1990).
[34] T. R. Waiters, R. S. Craig, and W. E. Wallace, Phys. Rev. **104**, 1240 (1956).
[35] A. Semenov, B. Günther, U. Böttger *et al.*, Phys. Rev. B **80**, 054510 (2009).
[36] Z. Zhou, G. Fricci, F. Mattioli, A. Gaggero, R. Leoni, S. Jahanmirinejad, T. B. Hoang, and A. Fiore, Phys. Rev. Lett. **110**, 133605 (2013).
[37] R. W. Heeres and V. Zwiller, Appl. Phys. Lett. **101**, 112603 (2012).
[38] F. Marsili, F. Najafi, E. Dauler *et al.*, Nano Lett. **11**, 2048 (2011).
[39] K. S. Il'in, M. Lindgren, M. Currie *et al.*, Appl. Phys. Lett. **76**, 2752 (2000).